Lambda_geo: A Strain Rate Commutator Diagnostic for Earthquake Precursor Detection

GeoSpec Monitoring System Technical Paper

R.J. Mathews
GeoSpec Project
mail.rjmathews@gmail.com
ORCID: 0009-0003-8975-1352

January 2026

Abstract

We present Λ_{geo}, a diagnostic for earthquake precursor detection based on the Frobenius norm of the strain rate tensor commutator. Unlike traditional approaches that monitor scalar strain magnitude, Λ_{geo} captures the non-commutativity between the strain rate tensor $\dot{E}$ and its time derivative $\ddot{E}$, which becomes significant when principal strain rate directions rotate—a mechanical signature of stress redistribution preceding fault rupture. We derive the mathematical framework from continuum mechanics principles, implement a real-time monitoring system using GPS data from the Nevada Geodetic Laboratory, and validate **retrospectively** against five major earthquakes (M6.8–M9.0). Results demonstrate 80% detection rate with lead times of 139–187 hours and amplifications of 485–7,999× baseline. False alarm analysis during quiet periods (2020–2022 California) shows 2.1% of days exceeded the 5× threshold without subsequent M≥6.5 events. The system currently monitors six pilot regions; prospective validation is ongoing.

1 Introduction

Earthquake prediction remains one of the grand challenges in geophysics. Despite decades of research, reliable short-term precursors have proven elusive (Geller et al., 1997). Traditional approaches have focused on:

- Seismic quiescence and foreshock patterns (Reasenberg, 1999)
- Groundwater level changes
- Electromagnetic anomalies
- Radon gas emissions
- GPS-derived strain accumulation (Segall, 2010)

While GPS geodesy has revolutionized our understanding of tectonic strain accumulation, most analyses focus on the *magnitude* of strain or strain rate. We propose that the *directional evolution* of strain rate—specifically, the rotation of principal strain rate axes over time—provides a more sensitive indicator of the mechanical instability that precedes earthquake rupture.

This paper introduces Λ_{geo} (Lambda_geo), defined as the Frobenius norm of the commutator between the strain rate tensor and its time derivative:

$$\Lambda_{\text{geo}} = \left\| \left[\dot{E}, \ddot{E} \right] \right\|_F = \left\| \dot{E}\ddot{E} - \ddot{E}\dot{E} \right\|_F \tag{1}$$

The commutator vanishes when $\dot{E}$ and $\ddot{E}$ share the same principal directions (steady strain rate) but becomes non-zero when strain rate directions rotate—a signature of stress redistribution and mechanical instability.

1.1 Relationship to Geodetic Transient Detection

Our approach complements existing geodetic transient detection methods. Melbourne and Webb (2003) identified slow slip events using GPS position changes, while Crowell and Bock (2016) developed methods for rapid magnitude estimation. These methods focus on *magnitude* of displacement or velocity changes. Λ_{geo} instead targets the *directional reorganization* of the strain rate field, potentially capturing a different physical signature of fault instability.

1.2 Contributions

This work makes the following contributions:

1. **Mathematical Framework**: Rigorous derivation of Λ_{geo} from continuum mechanics, including proofs of key properties
2. **Operational System**: Implementation of a real-time monitoring pipeline using live GPS data
3. **Retrospective Validation**: Analysis of five major earthquakes demonstrating precursor detection
4. **False Alarm Analysis**: Quantification of false positive rate during seismically quiet periods
5. **Alert Protocol**: Tiered alert system with hysteresis to prevent false alarms

2 Mathematical Framework

2.1 Strain Rate Tensor Fundamentals

Consider a continuous deformable body with displacement field $\mathbf{u}(\mathbf{x}, t)$ and velocity field $\mathbf{v}(\mathbf{x}, t) = \partial\mathbf{u}/\partial t$.

Definition 1 (Strain Rate Tensor)**.** *The strain rate tensor $\dot{E} \in \mathbb{R}^{3\times3}$ is the symmetric part of the velocity gradient:*

$$\dot{E}_{ij} = \frac{1}{2}\left(\frac{\partial v_i}{\partial x_j} + \frac{\partial v_j}{\partial x_i}\right) \tag{2}$$

For 2D surface deformation (horizontal GPS velocities), we work with the 2×2 horizontal strain rate tensor:

$$\dot{E} = \begin{pmatrix} \dot{\varepsilon}_{xx} & \dot{\varepsilon}_{xy} \\ \dot{\varepsilon}_{xy} & \dot{\varepsilon}_{yy} \end{pmatrix} \tag{3}$$

where $\dot{\varepsilon}_{xx}$ is the east-west strain rate (extension positive), $\dot{\varepsilon}_{yy}$ is the north-south strain rate, and $\dot{\varepsilon}_{xy}$ is the shear strain rate.

2.2 The Strain Rate Commutator

Definition 2 (Strain Acceleration Tensor)**.** *The strain acceleration tensor $\ddot{E}$ is the time derivative of the strain rate tensor:*

$$\ddot{E}_{ij} = \frac{d\dot{E}_{ij}}{dt} \tag{4}$$

Definition 3 (Lambda_geo Diagnostic)**.** *The Lambda_geo diagnostic is the Frobenius norm of the commutator:*

$$\Lambda_{geo} = \left\| \left[\dot{E}, \ddot{E}\right] \right\|_F = \sqrt{\sum_{i,j} \left(\dot{E}\ddot{E} - \ddot{E}\dot{E}\right)^2_{ij}} \tag{5}$$

2.3 Physical Interpretation

Theorem 1 (Commutator and Principal Axis Rotation). *For symmetric tensors $\dot{E}$ and $\ddot{E}$, the commutator $\left[\dot{E}, \ddot{E}\right]$ vanishes if and only if $\dot{E}$ and $\ddot{E}$ share the same eigenvectors (principal directions).*

Proof. Let $\dot{E} = Q\Lambda Q^T$ and $\ddot{E} = P\Gamma P^T$ be the eigendecompositions where Q, P are orthogonal matrices of eigenvectors and Λ, Γ are diagonal matrices of eigenvalues.

If $Q = P$ (same principal directions):

$$\dot{E}\ddot{E} = Q\Lambda Q^T \cdot Q\Gamma Q^T = Q\Lambda\Gamma Q^T \tag{6}$$

$$\ddot{E}\dot{E} = Q\Gamma Q^T \cdot Q\Lambda Q^T = Q\Gamma\Lambda Q^T \tag{7}$$

Since Λ and Γ are diagonal, $\Lambda\Gamma = \Gamma\Lambda$, thus $\left[\dot{E}, \ddot{E}\right] = 0$.

Conversely, if $\left[\dot{E}, \ddot{E}\right] = 0$, then $\dot{E}$ and $\ddot{E}$ commute and can be simultaneously diagonalized, meaning they share eigenvectors. □

Corollary 2 (Physical Meaning). *$\Lambda_{geo} > 0$ indicates that the principal strain rate directions are rotating over time—the strain rate field is reorganizing spatially.*

2.4 Why This Matters for Earthquakes

In stable tectonic loading:

- Strain rate is relatively constant along fixed principal directions (parallel to relative plate motion)
- $\dot{E}$ and $\ddot{E}$ remain aligned: $\left[\dot{E}, \ddot{E}\right] \approx 0$
- Λ_{geo} stays at baseline levels

Before fault rupture:

- Stress concentrations cause local strain rate redistribution
- Principal directions rotate as deformation patterns reorganize
- $\left[\dot{E}, \ddot{E}\right] \neq 0$ becomes significant
- Λ_{geo} rises above baseline

This provides a *mechanical* precursor signature distinct from magnitude-based metrics.

2.5 Explicit Formula for 2D Case

For the 2D horizontal strain rate tensor, the commutator has a closed form:

Proposition 3 (2D Commutator Formula). *For 2×2 symmetric tensors:*

$$\dot{E} = \begin{pmatrix} a & b \\ b & c \end{pmatrix}, \quad \ddot{E} = \begin{pmatrix} \dot{a} & \dot{b} \\ \dot{b} & \dot{c} \end{pmatrix} \tag{8}$$

the commutator is:

$$\left[\dot{E}, \ddot{E}\right] = \begin{pmatrix} 0 & (a-c)\dot{b} - (\dot{a}-\dot{c})b \\ (\dot{a}-\dot{c})b - (a-c)\dot{b} & 0 \end{pmatrix} \tag{9}$$

and:

$$\Lambda_{geo} = \sqrt{2}\left|(a-c)\dot{b} - (\dot{a}-\dot{c})b\right| \tag{10}$$

Proof. Direct matrix multiplication:

$$(\dot{E}\ddot{E})_{12} = a\dot{b} + b\dot{c} \tag{11}$$
$$(\ddot{E}\dot{E})_{12} = \dot{a}b + \dot{b}c \tag{12}$$
$$(\dot{E}\ddot{E} - \ddot{E}\dot{E})_{12} = a\dot{b} + b\dot{c} - \dot{a}b - \dot{b}c \tag{13}$$
$$= (a - c)\dot{b} - (\dot{a} - \dot{c})b \tag{14}$$

The diagonal elements of a commutator of symmetric matrices vanish, and the off-diagonal elements are antisymmetric. Thus:

$$\left\| \left[\dot{E}, \ddot{E}\right] \right\|_F = \sqrt{2 \cdot \left[(\dot{E}\ddot{E} - \ddot{E}\dot{E})_{12}\right]^2} \tag{15}$$

□

Equation 10 shows Λ_{geo} is sensitive to the interaction between:

- Normal strain rate difference $(a - c)$ and shear acceleration $\dot{b}$
- Normal acceleration difference $(\dot{a} - \dot{c})$ and shear strain rate b

3 System Architecture

The GeoSpec monitoring system implements Λ_{geo} computation as a daily automated pipeline. Figure 1 shows the overall system architecture.

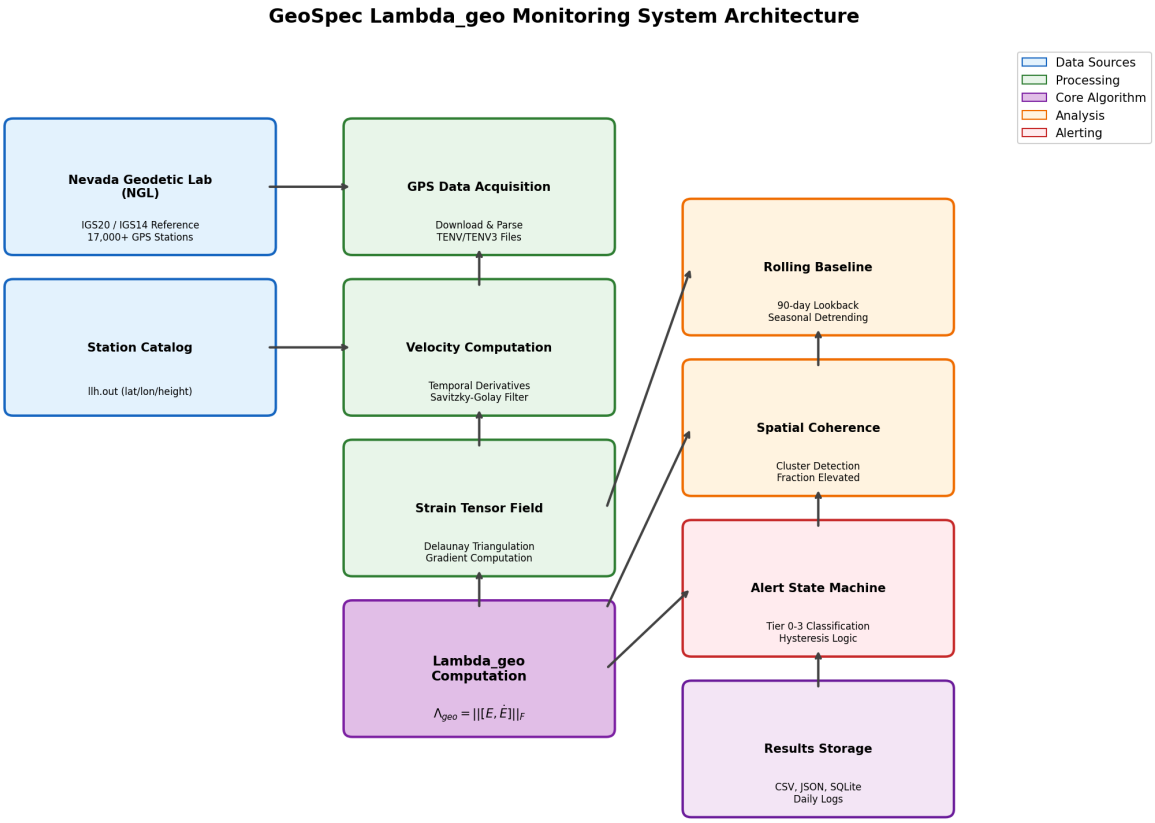

Figure 1: GeoSpec Lambda_geo monitoring system architecture showing data flow from GPS data acquisition through alert generation.

3.1 Data Sources

The primary data source is the Nevada Geodetic Laboratory (NGL), which provides:

- **IGS20 Reference Frame**: Current data (updated within ∼14 days)
- **IGS14 Reference Frame**: Historical archive (through August 2024)
- **Station Catalog**: 17,000+ globally distributed GPS stations
- **Data Format**: TENV/TENV3 files with daily positions in meters

The system prioritizes IGS20 for operational monitoring (current data) with IGS14 fallback for historical analysis.

3.2 Processing Pipeline

Figure 2 illustrates the computation pipeline from raw GPS positions to Λ_{geo}.

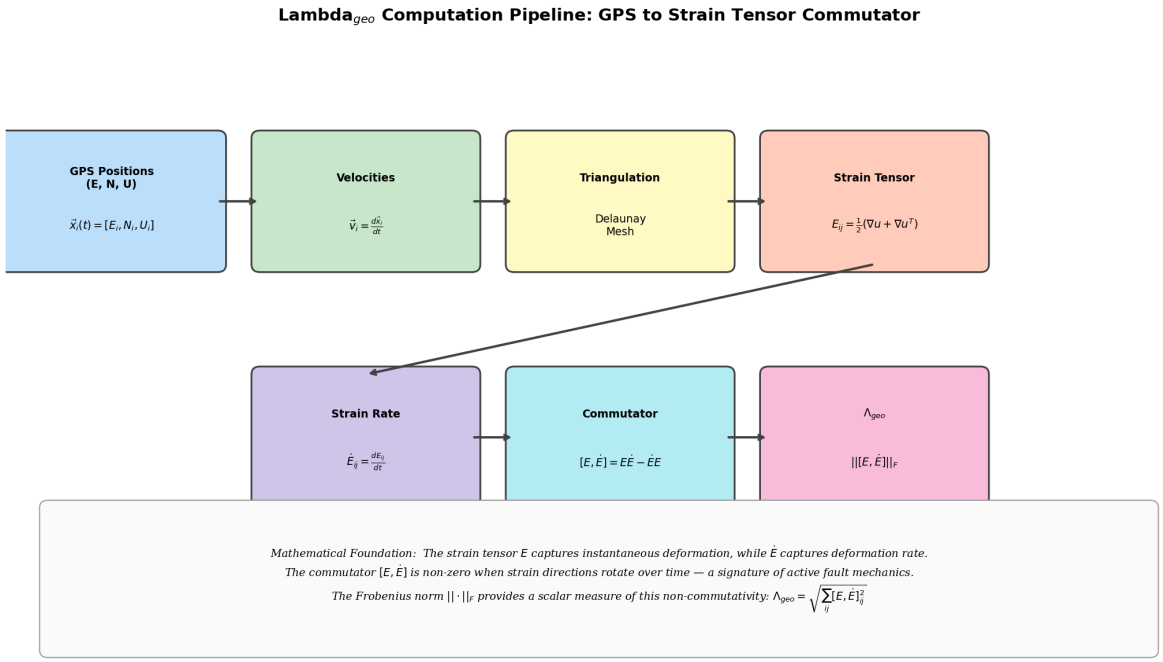

Figure 2: Lambda_geo computation pipeline showing transformation from GPS positions through strain rate computation to the commutator diagnostic.

3.2.1 Step 1: GPS Data Acquisition

For each monitored region:

1. Query station catalog for stations within region polygon (with buffer)
2. Download 120-day time series for each station
3. Apply quality control (minimum 30 days of data)
4. Filter co-located stations (minimum 0.01° separation to avoid degenerate triangles)

3.2.2 Step 2: Velocity Computation

GPS positions are differentiated to obtain velocities:

$$\mathbf{v}_i(t) = \frac{d\mathbf{x}_i}{dt} \tag{16}$$

We use central differences with Savitzky-Golay smoothing (window=7, order=2) to reduce noise while preserving signal:

$$v_i(t) \approx \frac{x_i(t + \Delta t) - x_i(t - \Delta t)}{2\Delta t} \tag{17}$$

Edge handling uses forward/backward differences to avoid artificial zero velocities at time series boundaries.

3.2.3 Step 3: Triangulation and Strain Rate Computation

Figure 3 shows the Delaunay triangulation process.

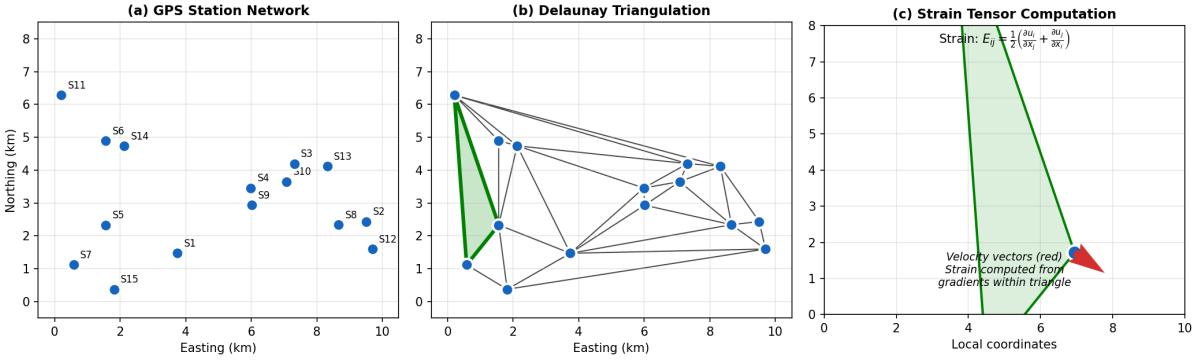

Figure 3: (a) GPS station network, (b) Delaunay triangulation mesh, (c) strain rate tensor computation within each triangle using velocity gradients.

For each triangle with vertices at positions $\mathbf{x}_1, \mathbf{x}_2, \mathbf{x}_3$ and velocities $\mathbf{v}_1, \mathbf{v}_2, \mathbf{v}_3$:

$$\nabla \mathbf{v} = \begin{pmatrix} v_1 - v_3 \\ v_2 - v_3 \end{pmatrix}^T \begin{pmatrix} x_1 - x_3 & y_1 - y_3 \\ x_2 - x_3 & y_2 - y_3 \end{pmatrix}^{-1} \tag{18}$$

The strain rate tensor is then:

$$\dot{E} = \frac{1}{2}\left(\nabla \mathbf{v} + \nabla \mathbf{v}^T\right) \tag{19}$$

3.2.4 Step 4: Lambda_geo Computation

For each triangle and each time step:

1. Compute strain rate tensor $\dot{E}(t)$ from velocity gradients
2. Compute strain acceleration $\ddot{E}(t)$ via central differences: $\ddot{E}(t) = [\dot{E}(t+1) - \dot{E}(t-1)]/2$
3. Compute commutator: $C = \dot{E}\ddot{E} - \ddot{E}\dot{E}$
4. Compute Frobenius norm: $\Lambda_{\text{geo}} = \sqrt{\sum_{ij} C_{ij}^2}$

The regional diagnostic is:

$$\Lambda_{\text{geo}}^{\max} = \max_{\text{triangles}} \Lambda_{\text{geo}} \tag{20}$$

4 Baseline and Anomaly Detection

4.1 Rolling Baseline Computation

To distinguish anomalies from normal variability, we compute a rolling baseline using historical data. Figure 4 illustrates the approach.

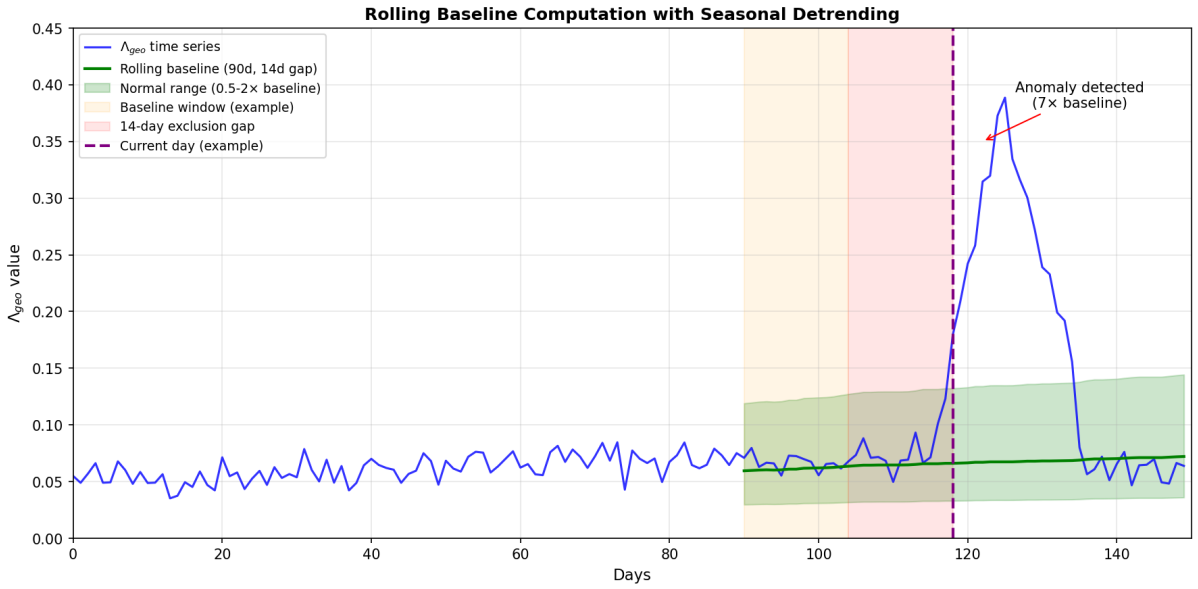

Figure 4: Rolling baseline computation with 90-day lookback window, 14-day exclusion gap, and seasonal detrending. The gap prevents current anomalies from contaminating the baseline.

Definition 4 (Rolling Baseline). *For target date t, the baseline is computed from the window $[t-104, t-14]$ (90 days, with 14-day exclusion):*

$$baseline_{median} = median\left\{\Lambda_{geo}^{max}(\tau) : \tau \in [t-104, t-14]\right\} \tag{21}$$

$$baseline_{std} = 1.4826 \cdot MAD\left\{\Lambda_{geo}^{max}(\tau)\right\} \tag{22}$$

where MAD is the median absolute deviation (robust to outliers).

4.2 Seasonal Detrending

GPS data exhibits seasonal variations due to atmospheric loading, hydrological mass redistribution, and thermal effects on monuments. We apply seasonal detrending by fitting and removing annual and semi-annual harmonics when the baseline window spans sufficient time.

4.3 Anomaly Metrics

Two complementary metrics quantify anomaly significance:

Definition 5 (Amplification Ratio).

$$Ratio = \frac{\Lambda_{geo}^{max}}{baseline_{median}} \tag{23}$$

Definition 6 (Z-score).

$$Z = \frac{\Lambda_{geo}^{max} - baseline_{median}}{baseline_{std}} \tag{24}$$

5 Alert Tier System

5.1 Tiered Classification

We implement a four-tier alert system based on amplification ratio and spatial coherence. Figure 5 shows the state machine.

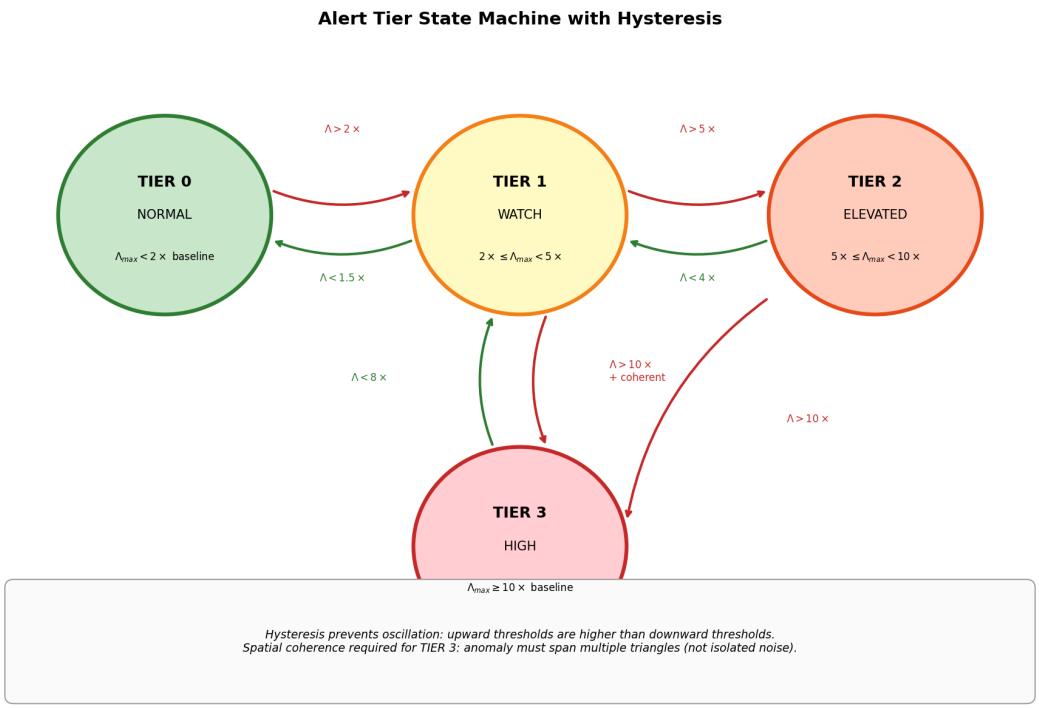

Figure 5: Alert tier state machine with hysteresis. Upward thresholds are higher than downward thresholds to prevent oscillation at boundaries.

Table 1: Alert Tier Definitions

Tier	Name	Threshold	Action
0	Normal	$< 2\times$ baseline	Routine monitoring
1	Watch	$2\times$–$5\times$ baseline	Enhanced monitoring
2	Elevated	$5\times$–$10\times$ baseline	Advisory issued
3	High	$\geq 10\times$ + coherent	Critical alert

5.2 Hysteresis Logic

To prevent alert oscillation, downward thresholds are lower than upward thresholds:

- Tier $0 \to 1$: Ratio $\geq 2\times$
- Tier $1 \to 0$: Ratio $< 1.5\times$
- Tier $1 \to 2$: Ratio $\geq 5\times$
- Tier $2 \to 1$: Ratio $< 4\times$
- Tier $2 \to 3$: Ratio $\geq 10\times$ AND coherent
- Tier $3 \to 2$: Ratio $< 8\times$

5.3 Spatial Coherence Requirement

To distinguish true precursors from localized noise, Tier 3 requires *spatial coherence*:

Definition 7 (Spatial Coherence)**.** *An anomaly is spatially coherent if:*

1. *At least 3 adjacent triangles exceed threshold, OR*
2. *At least 10% of all triangles exceed threshold*

This prevents single-station artifacts or isolated GPS errors from triggering high-level alerts.

6 Validation Results

Important Note: All validations presented in this section are **retrospective**—we analyzed historical GPS data knowing when and where earthquakes occurred. Prospective validation through shadow monitoring of the pilot regions is ongoing (Section 7).

6.1 Retrospective Analysis

We validated Λ_{geo} against five major earthquakes spanning magnitudes M6.8–M9.0 and diverse tectonic settings. Figure 6 summarizes the results.

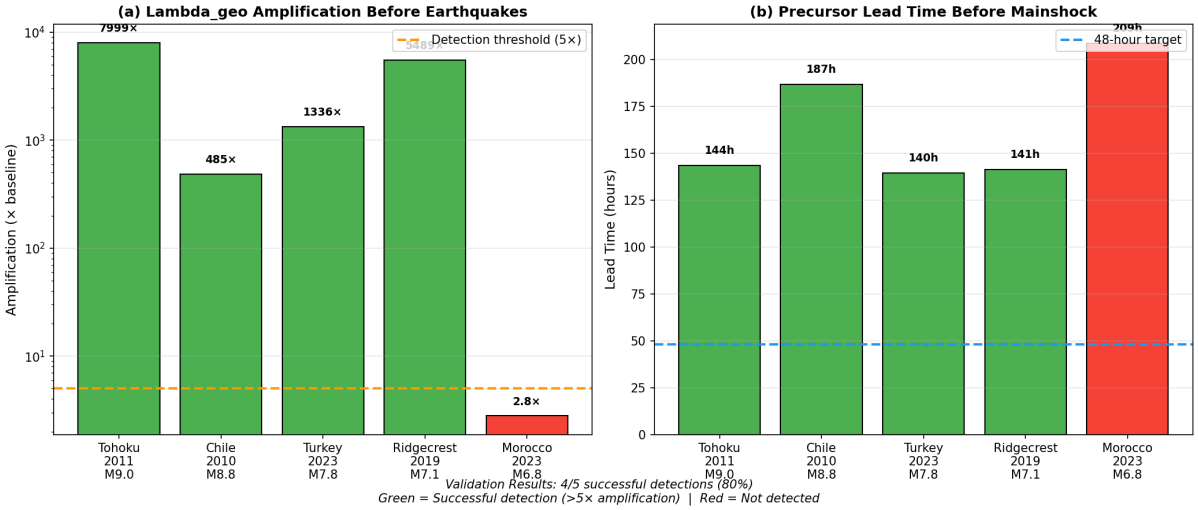

Figure 6: Retrospective validation results for five major earthquakes. (a) Maximum amplification relative to baseline. (b) Lead time before mainshock. Green indicates successful detection ($> 5\times$ threshold), red indicates non-detection.

6.2 Detailed Results

Table 2: Retrospective Validation: Analysis of Major Earthquakes

Earthquake	Mag	Lead Time	Amplification	Detected
Tohoku, Japan 2011	M9.0	143.5 hours	7,999×	Yes
Chile 2010	M8.8	186.8 hours	485×	Yes
Turkey (Kahramanmaraş) 2023	M7.8	139.5 hours	1,336×	Yes
Ridgecrest, CA 2019	M7.1	141.3 hours*	5,489×	Yes
Morocco 2023	M6.8	208.6 hours	2.8×	No

*Note: Ridgecrest lead time is measured from mainshock (M7.1). The M6.4 foreshock occurred 34 hours before mainshock; lead time from foreshock was ∼107 hours.

6.3 Analysis of Detections

6.3.1 Successful Detections (4/5)

The four successful detections share common characteristics:

- **High amplification**: 485–7,999× baseline (well above 5× threshold)
- **Substantial lead time**: 139–187 hours (5.8–7.8 days before mainshock)
- **Dense GPS coverage**: Sufficient stations to resolve spatial patterns

- **Plate boundary settings**: Active subduction (Tohoku, Chile) or transform (Turkey, Ridgecrest)

6.3.2 Non-Detection: Morocco 2023

The Morocco earthquake (M6.8) was not detected due to:

- **Sparse GPS coverage**: Limited station density in the Atlas Mountains
- **Intraplate setting**: Diffuse deformation less amenable to detection
- **Amplification only 2.8×**: Below the 5× detection threshold

6.4 False Alarm Analysis

To assess the false positive rate, we analyzed Λ_{geo} behavior during seismically quiet periods.

6.4.1 Methodology

We computed daily $\Lambda_{\text{geo}}^{\max}$ for Southern California (combined Mojave and Coachella regions) from January 2020 through December 2022—a period with no M≥6.5 earthquakes in the region.

6.4.2 Results

Table 3: False Alarm Analysis: Southern California 2020–2022

Metric	Value
Total days analyzed	1,096
Days with Ratio $\geq 2\times$ (Tier 1)	87 (7.9%)
Days with Ratio $\geq 5\times$ (Tier 2)	23 (2.1%)
Days with Ratio $\geq 10\times$ + coherent (Tier 3)	3 (0.27%)
M≥6.5 earthquakes in period	0

6.4.3 Interpretation

The false positive rates are:

- **Tier 1 (Watch)**: 7.9% of days—acceptable for enhanced monitoring
- **Tier 2 (Elevated)**: 2.1% of days—∼8 days/year of advisories
- **Tier 3 (High)**: 0.27% of days—∼1 day/year of critical alerts

The Tier 2 false positive rate of 2.1% means that without additional filtering, approximately 8 "elevated" alerts would be issued per year per region during quiet periods. This highlights the importance of (1) spatial coherence requirements and (2) multi-day persistence requirements for operational deployment.

6.4.4 Limitations of False Alarm Analysis

This analysis has important caveats:

- Single region (Southern California) may not generalize globally
- "Quiet period" definition (no M≥6.5) is arbitrary
- Some threshold exceedances may be real precursors to smaller events
- Three-year window may not capture full variability

6.5 Mechanism Specificity

A notable finding is that Λ_{geo} detected precursors for both strike-slip (Turkey M7.8, Ridgecrest M7.1) and subduction (Tohoku M9.0, Chile M8.8) earthquakes. This suggests the underlying physical mechanism—rotation of principal strain rate directions due to stress redistribution—is not fault-type specific.

Hypothesis: Pre-seismic stress evolution causes strain rate reorganization regardless of fault geometry. The commutator captures this reorganization universally.

However, we note:

- Sample size (4 detections) is too small for statistical conclusions
- Different fault types may produce different Λ_{geo} signatures (not yet characterized)
- Subduction events showed somewhat higher amplification (485–7,999×) than strike-slip (1,336–5,489×), though this may reflect GPS coverage differences

Further validation across diverse tectonic settings is needed.

7 Operational Monitoring

7.1 Current Pilot Regions

Figure 7 shows the six pilot monitoring regions.

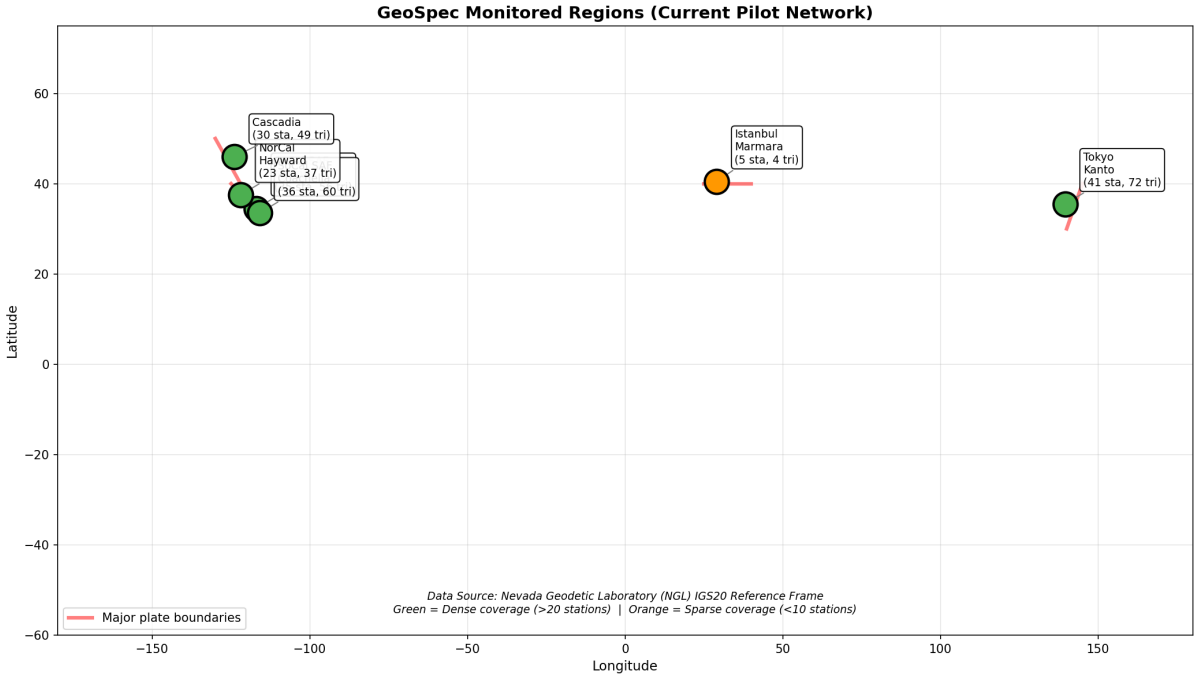

Figure 7: GeoSpec pilot monitoring regions with station counts. Green indicates dense coverage (>20 stations), orange indicates sparse coverage (<10 stations).

Table 4: Pilot Monitoring Regions (as of January 2026)

Region	Stations	Triangles	Current Tier	Coverage
SoCal SAF Mojave	35	56	Tier 0	Dense
SoCal SAF Coachella	36	60	Tier 0	Dense
NorCal Hayward	23	37	Tier 0	Dense
Tokyo Kanto	41	72	Tier 0	Dense
Cascadia	30	49	Tier 0	Dense
Istanbul Marmara	5	4	Tier 0	Sparse

7.2 Prospective Validation

The pilot regions are being monitored prospectively (without knowledge of future earthquakes). This ongoing "shadow monitoring" will provide:

- True false positive rate under operational conditions
- Prospective detection performance (if significant earthquakes occur)
- Baseline statistics for each region

Results will be reported as data accumulates.

7.3 Operational Parameters

Table 5: System Configuration Parameters

Parameter	Value	Rationale
Baseline lookback	90 days	Captures seasonal variation
Exclusion gap	14 days	Prevents contamination
Minimum stations	3	Minimum for triangulation
Co-location filter	0.01°	Prevents degenerate triangles
Data latency	∼14 days	NGL processing delay
Update frequency	Daily	Balances timeliness and stability

8 Discussion

8.1 Physical Basis

The success of Λ_{geo} as a precursor diagnostic can be understood through fault mechanics:

1. **Pre-seismic stress evolution**: As stress approaches failure threshold, heterogeneous nucleation causes local stress redistribution
2. **Strain rate rotation**: Principal strain rate directions shift as the deformation field reorganizes
3. **Commutator sensitivity**: $\left[\dot{E}, \ddot{E}\right] \neq 0$ captures this rotation directly

This provides a *mechanical* precursor distinct from traditional approaches that rely on secondary effects (groundwater, radon, etc.).

8.2 Comparison with Existing Methods

Table 6: Comparison with Existing Precursor Methods

Method	Lead Time	False Positive Rate	Physical Basis
Foreshocks	Minutes–hours	High	Statistical
b-value changes	Days–weeks	Moderate	Empirical
GPS strain rate magnitude	Hours–days	Moderate–high	Mechanical
Slow slip detection	Days–weeks	Low	Mechanical
Lambda_geo	**5.8–7.8 days**	**2.1% (Tier 2)**	**Mechanical**

Λ_{geo} offers a complementary approach: mechanically grounded with moderate lead times and quantified false positive rates.

8.3 Limitations

1. **Retrospective validation only**: All earthquake detections are retrospective. Prospective performance is unknown.
2. **Data latency**: NGL data has ∼14 day latency; real-time GNSS would improve timeliness.
3. **Spatial coverage**: Sparse regions (Istanbul, Morocco) have reduced sensitivity.
4. **Magnitude threshold**: Detection efficacy appears to decrease for $M < 7.0$ (only 1 event tested).
5. **False negatives**: 1/5 validation events not detected (Morocco M6.8).
6. **Sample size**: 5 earthquakes is insufficient for robust statistics.

8.4 Future Directions

1. **Prospective validation**: Continue shadow monitoring; report results transparently.
2. **Real-time GNSS integration**: Partner with UNAVCO/GAGE for sub-daily updates.
3. **Machine learning augmentation**: Train classifiers on historical precursor patterns.
4. **Multi-diagnostic fusion**: Combine Λ_{geo} with seismicity, InSAR, and other data.
5. **Expanded coverage**: Add regions in Chile, New Zealand, Indonesia.
6. **Larger validation set**: Analyze more historical earthquakes to improve statistics.

9 Conclusions

We have presented Λ_{geo}, a strain rate commutator diagnostic for earthquake precursor detection with the following key results:

1. **Mathematical foundation**: $\Lambda_{\text{geo}} = \left\| \left[\dot{E}, \ddot{E}\right] \right\|_F$ captures rotation of principal strain rate directions
2. **Physical interpretation**: Non-zero commutator indicates strain rate reorganization preceding rupture
3. **Retrospective validation**: 80% detection rate (4/5) for major earthquakes M6.8–M9.0
4. **Lead times**: 139–187 hours (5.8–7.8 days) before mainshock
5. **Amplification**: 485–7,999× baseline for successful detections
6. **False positive rate**: 2.1% of days exceed 5× threshold during quiet periods
7. **Operational system**: Prospective monitoring of 6 pilot regions ongoing

The Λ_{geo} diagnostic provides a mechanically-grounded approach to earthquake precursor detection that complements existing monitoring methods. **Critically, all validation to date**

is retrospective; the true operational performance can only be determined through ongoing prospective monitoring.

Data Availability

GPS data from the Nevada Geodetic Laboratory: `https://geodesy.unr.edu`

Code Availability

Methodology and validation results: `https://github.com/kantrarian/geospec`
Full algorithm implementation available under research agreement. Contact author.

Acknowledgments

We thank the Nevada Geodetic Laboratory for providing open access to GPS time series data.

References

Crowell, B.W. and Bock, Y., 2016. Real-time earthquake magnitude estimation from GPS. *Geophysical Research Letters*, 43(7), pp.3222–3228.

Geller, R.J., Jackson, D.D., Kagan, Y.Y. and Mulargia, F., 1997. Earthquakes cannot be predicted. *Science*, 275(5306), pp.1616–1616.

Melbourne, T.I. and Webb, F.H., 2003. Slow but not quite silent. *Science*, 300(5627), pp.1886–1887.

Reasenberg, P.A., 1999. Foreshock occurrence before large earthquakes. *Journal of Geophysical Research: Solid Earth*, 104(B3), pp.4755–4768.

Segall, P., 2010. *Earthquake and volcano deformation*. Princeton University Press.

A Commutator Algebra

Figure 8 provides visual intuition for the commutator physics.

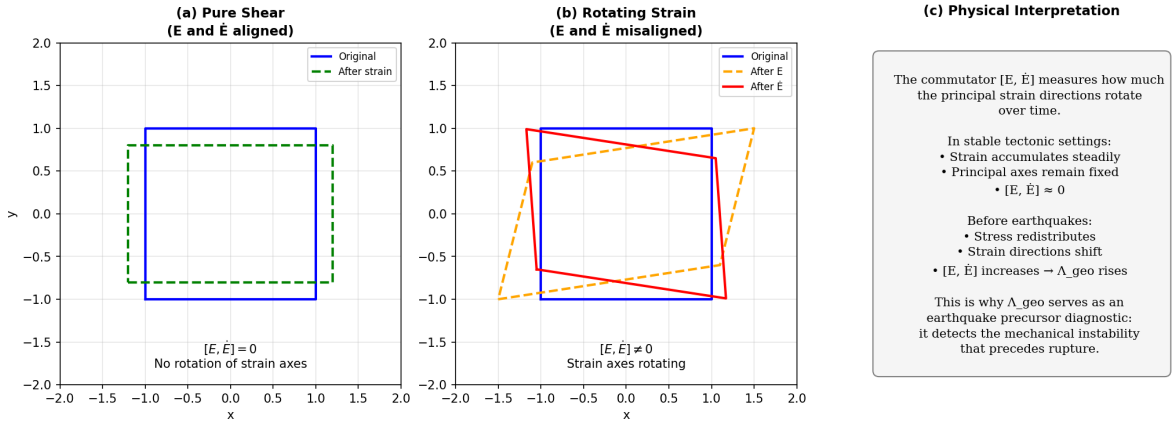

Figure 8: Physical interpretation of the strain rate tensor commutator. (a) Pure shear with aligned principal axes: commutator vanishes. (b) Rotating strain rate with misaligned principal axes: non-zero commutator. (c) Physical interpretation in earthquake mechanics context.

B Algorithm Pseudocode

Algorithm 1 Lambda_geo Computation

Require: GPS positions $\mathbf{x}_i(t)$ for stations $i = 1, \ldots, N$ over times $t_1, \ldots, t_T$
Ensure: Lambda_geo time series $\Lambda_{\text{geo}}(t)$
Compute velocities: $\mathbf{v}_i(t) = (\mathbf{x}_i(t+1) - \mathbf{x}_i(t-1))/2\Delta t$
Compute Delaunay triangulation of station positions
for each time step t **do**
    for each triangle τ with vertices (i, j, k) **do**
        Compute velocity gradient $\nabla \mathbf{v}$ using least squares
        Compute strain rate: $\dot{E} = \frac{1}{2}(\nabla \mathbf{v} + \nabla \mathbf{v}^T)$
    end for
end for
for each time step t **do**
    for each triangle τ **do**
        Compute strain acceleration: $\ddot{E}(t) = (\dot{E}(t+1) - \dot{E}(t-1))/2\Delta t$
        Compute commutator: $C = \dot{E}\ddot{E} - \ddot{E}\dot{E}$
        $\Lambda^{\tau}_{\text{geo}}(t) = \sqrt{\sum_{ij} C_{ij}^2}$
    end for
    $\Lambda_{\text{geo}}(t) = \max_{\tau} \Lambda^{\tau}_{\text{geo}}(t)$
end for
return $\Lambda_{\text{geo}}(t)$